THE EFFECTS OF HIGH DUCTILE STRUCTURES WITH EMBEDDED FOUNDATION INCLUDING SOIL-STRUCTURE INTERACTION

ITO Shinji[1], YAMASHITA Tadamichi[2], SHIRAYAMA Atsuko[3] and KENSUKE Baba[4]

[1] *Division of Global Architecture, Graduate School of Engineering, Osaka University*
[2] *KOZO KEIKAKU ENGINEERING Inc.*
[3] *General Building Research Corporation of Japan*
[4] *Associate Professor, Division of Global Architecture, Graduate School of Osaka University*
Email: shin_ji@d3.dion.ne.jp

ABSTRACT:

Seismic behaviors are evaluated when high ductile structures are supported by embedded foundation and interactive with their surrounding soil ground. Transfer functions are defined on the face of embedded foundation with sway and rocking motions. Physical parameters are selected out of various properties of interaction systems to investigate response behaviors such as ductility factors and natural periods of upper structure, as well as embedment depth and shear wave velocities of soil ground. Response measurement indexes are adopted among yield shear force, seismic input energy, radiation damping energy and cumulative plastic deformation for upper structures and base foundation excited with significant seismic motions. Effect of dynamic soil-structure interaction is consequently confirmed for high ductile structures supported with embedded foundation.

KEYWORDS: Soil-structure interaction, radiation damping, high ductile structure and embedded foundation

1. INTRODUCTION

Soil-structure interaction phenomena are generally considered effective to decrease upper structural response in an elastic range but not always expected in an elasto-plastic range under seismic excitations. Interactive energy dissipation properties are greatly influenced with natural period of structures, size of foundations, type of soils and especially with maximum ductility response of upper structures.
To evaluate the structural performance under significant seismic motion, it is necessary to build a dynamic interaction system that upper-structures are assumed to behave in an elasto-plasticity range. However, the factors of structural damages have not been explained accurately yet, a lot of relating parameters. Moreover, the high ductile design building is extending with the development of various structural materials. In the last report [1], useful findings about the soil-structure interaction not buried were obtained. In this paper, to investigate such structure models with burial of base and to verify the plasticity influence on soil-structure interaction phenomenon.

2. ANALYTICAL PROCEDURE

2.1 Equation of Motion

In this study, a soil-structure interaction model is built on one-story upper-structure with the cubic rectangle foundation in an elastic half space [2]. The dynamic system is divided into upper structure-foundation and elastic half space. Transfer functions are set on their interfaces of horizontal direction and rotational one [3], along. The following procedure is adopted to carry out the step-by-step method integrated along time axis.

Equations of motions are expressed with Eq.(1) in frequency domain for sway-rocking model by using lateral component $\tilde{\boldsymbol{x}}(\omega)$ of upper structure and sustained base foundation.

$$\left(-\omega^2\boldsymbol{M}+i\omega\boldsymbol{C}+\boldsymbol{K}\right)\tilde{\boldsymbol{x}}(\omega)=\omega^2\boldsymbol{M}\,\boldsymbol{e}\,\tilde{u}_G(\omega)-\tilde{\boldsymbol{H}}(\omega)\tilde{\boldsymbol{x}}(\omega)\quad :\boldsymbol{e}=(1,\cdots,1)^T\,, \tag{1}$$

in which $\boldsymbol{M}$, $\boldsymbol{C}$ and $\boldsymbol{K}$ are the matrices of mass, damping and stiffness for upper structures and base ones respectively, $\tilde{u}_G(\omega)$ denotes the lateral component of seismic excitations, $\tilde{\boldsymbol{H}}(\omega)$ means the transfer function matrix and i is the imaginary unit. On the contrary, Eq.(1) can be rewritten with integro-differential formula in the time-domain.

$$\boldsymbol{M}\,\ddot{\boldsymbol{x}}(t)+\boldsymbol{C}\,\dot{\boldsymbol{x}}(t)+\boldsymbol{K}\,\boldsymbol{x}(t)=-\boldsymbol{M}\,\boldsymbol{e}\,\ddot{u}_G(t)-\boldsymbol{H}(t)*\boldsymbol{x}(t). \tag{2}$$

The symbol (*) corresponds to the convolution integral. In addition, by using delta function $\delta^{(m)}(t-\tau_n)$ which contains differentiation m and delay time τ_n, transfer function matrix $\boldsymbol{H}(t)$ is obtained in the time-domain to avoid the convolution integral and expressed as Eq. (3).

$$\boldsymbol{H}(t)=\sum_{m=0}^{M}\sum_{n=0}^{N}\delta^{(m)}(t-\tau_n)\boldsymbol{D}_{mn} \quad : \quad \tau_n \ge 0\,. \tag{3}$$

The symbol m is associated with time differentiation at the symbol n with time delay. The matrix $\boldsymbol{D}_{mn}$ corresponds to coefficients in the real domain. The differentiation time m is limited to two times for the delta function and the Eq.(4) is obtained in consideration of the structure nonlinearity.

$$\boldsymbol{M}\,\ddot{\boldsymbol{x}}(t)+\boldsymbol{C}\,\dot{\boldsymbol{x}}(t)+\boldsymbol{f}(\boldsymbol{x}(t),t)+\sum_{m=0}^{2}\sum_{n=0}^{N}\boldsymbol{D}_{mn}\,\boldsymbol{x}^{(m)}(t-\tau_n)=-\boldsymbol{M}\,\boldsymbol{e}\,\ddot{u}_G(t)\,. \tag{4}$$

The vector $\boldsymbol{f}(\boldsymbol{x}(t),t)$ means hysteresis characteristics. It is possible to apply step-by-step integration method to Eq.(4) when upper-structure model has a usual hysteresis loop.

2.2 Transfer Function

The frequency function of *Dynamical Ground Compliance* (*D.G.C.*) is chosen as transfer function at the bottom of foundation and *Novak* function [4] is chosen as transfer function at the side of foundation. On the free surface of elastic half space with homogeneous and isotropic properties, *D.G.C.* function is defined in the ratio between the displacement responses and the stress excitations spreading over the rectangular base portion of the surface. *D.G.C.* function is obtained in accordance with the average energy method [5] and converted into the inverse impedance function.

The impedance coefficient matrix $\boldsymbol{D}_{mn}$ is obtained by the following procedures to compose Eq.(3) in the time domain.

(1) *D.G.C.* functions are numerically converted into impedance functions.

(2) The impedance coefficient matrix $\boldsymbol{D}_{mn}$ is obtained through the simulation procedure for the frequency function $\tilde{\boldsymbol{H}}(\omega)$ of Eq.(5).

$$\tilde{\boldsymbol{H}}(\omega)=\sum_{m=0}^{2}\sum_{n=0}^{N}(i\omega)^{m}\exp(-i\omega\tau_n)\boldsymbol{D}_{mn}\,, \tag{5}$$

$$\tilde{\boldsymbol{H}}(\omega)=\begin{bmatrix}\tilde{h}_R(\omega) & & & \\ & \tilde{h}_H(\omega) & & \\ & & 0 & \\ & & & \ddots & \\ & & & & 0\end{bmatrix},\quad \boldsymbol{D}_{mn}=\begin{bmatrix}d_{mn}^{R} & & & \\ & d_{mn}^{H} & & \\ & & 0 & \\ & & & \ddots & \\ & & & & 0\end{bmatrix}, \tag{6}$$

$$\tilde{h}^{R}(\omega)={}_{D}\tilde{h}^{R}(\omega)+{}_{N}\tilde{h}^{R}(\omega), \tag{7}$$

$$\tilde{h}^{H}(\omega)={}_{D}\tilde{h}^{H}(\omega)+{}_{N}\tilde{h}^{H}(\omega), \tag{8}$$

$$d_{mn}^{R}={}_{D}d_{mn}^{R}+{}_{N}d_{mn}^{R}\,, \tag{9}$$

$$d_{mn}^{H}={}_{D}d_{mn}^{H}+{}_{N}d_{mn}^{H}\,. \tag{10}$$

The real factors ${}_D d^R_{mn}$, ${}_D d^H_{mn}$, ${}_N d^R_{mn}$ and ${}_N d^H_{mn}$ are expanded in series through the transfer functions of *D.G.C.* and the ones of *Novak*. The time delay of a delta function is limited to two steps in the simulations of the transfer functions $\tilde{\boldsymbol{H}}(\omega)$ because simulation results are obtained with good accuracy. Table 1, 2 show the simulation results with *Poisson's ratio* $\nu = 0.40$.

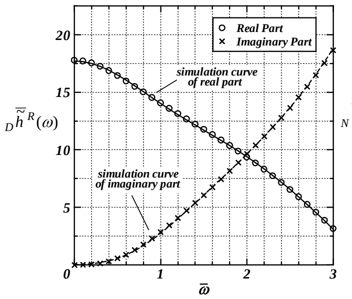

Figure 1.1
D.G.C. function

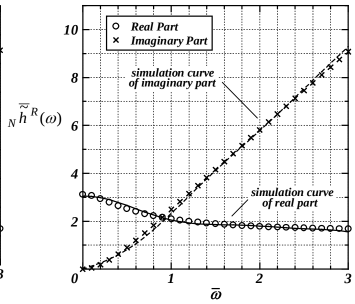

Figure 1.2
Novak function

Figure 1. Simulation of Rotation

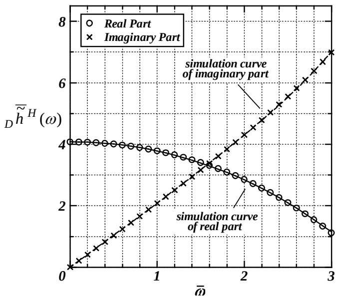

Figure 2.1
D.G.C. function

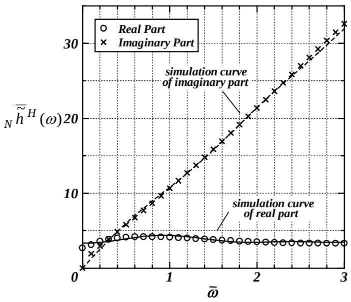

Figure 2.2
Novak function

Figure 2. Simulation of Horizontal Translation

$$\bar{\tilde{h}}^R(\varpi) = \bar{d}_{00} + (i\,\varpi)^2 \bar{d}_{20} + \bar{d}_{01}\cos\varpi\tau_1 + \varpi\bar{d}_{11}\sin\varpi\tau_1 + (i\,\varpi)^2 \bar{d}_{21}\cos\varpi\tau_1$$
$$+ \bar{d}_{02}\cos\varpi\tau_2 + \varpi\bar{d}_{12}\sin\varpi\tau_2 + (i\varpi)^2\bar{d}_{22}\cos\varpi\tau_2$$
$$\bar{\tilde{h}}^I(\varpi) = \varpi\bar{d}_{10} - \bar{d}_{01}\sin\varpi\tau_1 + \varpi\bar{d}_{11}\cos\varpi\tau_1 - (i\varpi)^2\bar{d}_{21}\sin\varpi\tau_1$$
$$- \bar{d}_{02}\sin\varpi\tau_2 + \varpi\bar{d}_{12}\cos\varpi\tau_2 - (i\varpi)^2\bar{d}_{22}\sin\varpi\tau_2$$

Table 1. Dimensionless Coefficients in the Impedance Functions of Rotation

Table 1.1 D.G.C. function

${}_D\bar{d}^R_{00}$	12.1958	${}_D\bar{d}^R_{01}$	5.3037	${}_D\bar{d}^R_{02}$	0.2023
${}_D\bar{d}^R_{10}$	7.1260	${}_D\bar{d}^R_{11}$	2.2608	${}_D\bar{d}^R_{12}$	-0.0447
${}_D\bar{d}^R_{20}$	0.2727	${}_D\bar{d}^R_{21}$	0.8872	${}_D\bar{d}^R_{22}$	0.0374

Table 1.2 Novak function

${}_N\bar{d}^R_{00}$	1.5287	${}_N\bar{d}^R_{01}$	1.4528	${}_N\bar{d}^R_{02}$	0.0780
${}_N\bar{d}^R_{10}$	3.4094	${}_N\bar{d}^R_{11}$	0.4419	${}_N\bar{d}^R_{12}$	-0.0759
${}_N\bar{d}^R_{20}$	-0.1400	${}_N\bar{d}^R_{21}$	0.2905	${}_N\bar{d}^R_{22}$	0.0190

Table 2. Dimensionless Coefficients in the Impedance Functions of Horizontal Translation

Table 2.1 D.G.C. function

${}_D\bar{d}^H_{00}$	3.6305	${}_D\bar{d}^H_{01}$	0.4618	${}_D\bar{d}^H_{02}$	-0.0126
${}_D\bar{d}^H_{10}$	2.4623	${}_D\bar{d}^H_{11}$	0.3120	${}_D\bar{d}^H_{12}$	0.0028
${}_D\bar{d}^H_{20}$	0.1711	${}_D\bar{d}^H_{21}$	0.0914	${}_D\bar{d}^H_{22}$	-0.0013

Table 2.2 Novak function

${}_N\bar{d}^H_{00}$	5.2116	${}_N\bar{d}^H_{01}$	-1.6906	${}_N\bar{d}^H_{02}$	-0.1950
${}_N\bar{d}^H_{10}$	9.8652	${}_N\bar{d}^H_{11}$	-0.6172	${}_N\bar{d}^H_{12}$	0.2339
${}_N\bar{d}^H_{20}$	0.3521	${}_N\bar{d}^H_{21}$	-0.5308	${}_N\bar{d}^H_{22}$	-0.0688

The dimensionless parameters are adopted with the over script (-),

$$\bar{d}^R_{mn} = 3\,d^R_{mn}\,\frac{\omega^m_G}{Gb^3}\,, \tag{11}$$

$$\bar{d}^H_{mn} = d^H_{mn}\,\frac{\omega^m_G}{Gb}\,, \tag{12}$$

$$\varpi = \frac{\omega}{\omega_G}, \varpi_L = \frac{\omega_L}{\omega_G} = 2, \tau_n = \frac{n\pi}{\omega_L}, \omega_G = \frac{1}{b}\sqrt{\frac{G}{\rho}}\,,$$

in which half width b is given for base foundation while shear stiffness G and mass density ρ for soil ground, respectively.

2.3 Analytical Models and Physical Parameters

The following descripts are defined for analytical models and parameters.

Upper-Structure

(1) Structural model is targeted in shearing type and constructed with one horizontal degree of freedom. Multi-story structure is assumed with uniform distributed masses and constant heights of floor. Equivalent systems are, however, used to have one degree of freedom because the first mode shape is confined *reverse-triangle* for upper structure.
(2) The first natural period T_1 is set inside the range of 0.1-2.0 second for upper structures treated in elastic.
(3) The mass is 9.8(kN/m^2) and the half width is 20(m) for each floor shaped square.
(4) The total height is set to be T/0.025(m) while each floor height is 4.0(m) for structural model. Equivalent mass and equivalent height are consequents calculated for one mass upper structure.
(5) The stiffness is decided out of the first natural period T_1 for upper structure.
(6) The hysteretic characteristics are assumed bi-linear, with secondary stiffness factor $\zeta = 0.20$ compared with the initial stiffness.
(7) Internal damping is set proportional to the initial stiffness proportional, and the damping ratio is 0.01 for the first mode of upper-structure.
(8) The maximum response ductility factors μ is 1.5, 3.0 and 5.0 cases for the upper-structure models under the input earthquake motion.

Yield shear strength is calculated by the convergence operation [6] based on the secant method to the maximum response of ductility rate around the set value of μ. The error is less than 1% between the set value and the response one.

Square Rigid Foundation

(1) Half width b is assumed to be 20(m).
(2) The embedment depth is assumed among three kinds of 0(m), 12(m), and 24(m).
(3) The base mass is assumed to be 58.8(kN/m^2) at 0(m), 176.4(kN/m^2) at 12(m) and 294(kN/m^2) at 24(m) in embedment depth.

Infinite Elastic Half Ground

(1) The mass density ρ is assumed to be 1800(kg/m^3).
(2) The shear wave velocity Vs (=$\sqrt{G/\rho}$) is adopted with 360,300,240,180,120(m/s).

The *Newmark's-β* method (β = 1/4) is applied to the numerical analysis, in which the time step Δt is 0.002(s) through step by step way. The original quake wave of BCJ-L2 (made by the Building Center of Japan) is used for the input seismic motion.

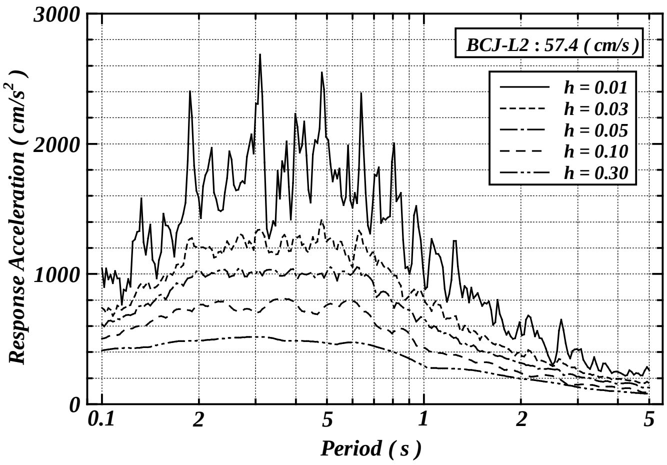

Figure 3. Acceleration response spectrum of input seismic motion

3.EVALUATING INDEX

The response index α_y is defined to evaluate the yield story shear force Q_y, as follows.

$$\alpha_y = Q_y / M \cdot g \, , \qquad (13)$$

in which M is the effective mass of the upper-structure, and g is gravity acceleration.
The equivalent velocity V_I is given in Eq.(14) for energy E_I coming into upper-structure model.

$$V_I = \sqrt{2 \cdot E_I / M} \; . \qquad (14)$$

The energy ratio W_H/E_I is also used for hysteretic damping energy W_H absorbing in upper-structure model. The radiation damping energy W_R is defined to escape for soil ground as follows,

$$W_R = E_I - \left(W_H + W_C + W_E\right), \qquad (15)$$

in which W_C means viscous damping energy as well as W_E total amounts of kinetic energy and potential one in upper-structure model.
In addition cumulative plastic deformation ratio, η is defined as follows, when estimating a safety rate of aseismic performance of upper-structure.

$$\eta = X_p / d_y \, , \qquad (16)$$

in which X_P and d_y mean cumulative plastic deformation and yield displacement.

4. SEISMIC RESPONSE CHARACTERISTICS

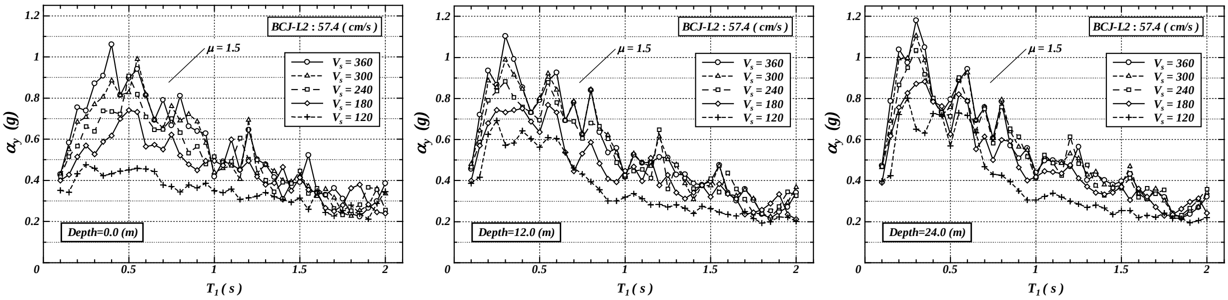

Figure 4.1.1 Depth=0(m) Figure 4.1.2 Depth=12(m) Figure 4.1.3 Depth=24(m)

Figure 4.1 Yield shear force coefficient (μ =1.5)

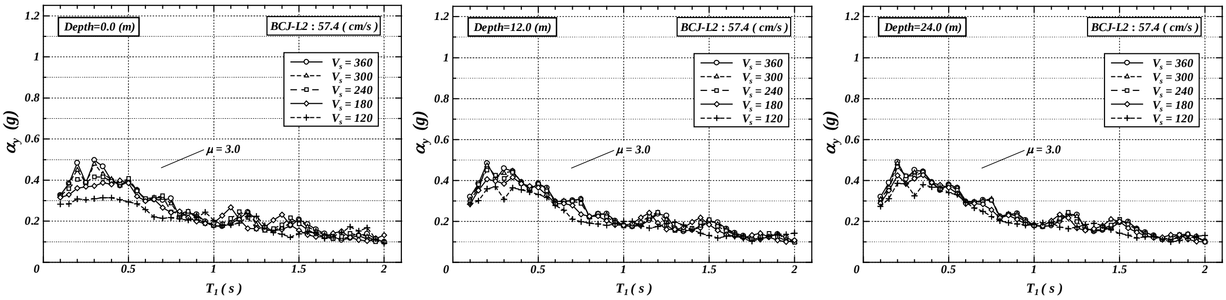

Figure 4.2.1 Depth=0(m) Figure 4.2.2 Depth=12(m) Figure 4.2.3 Depth=24(m)

Figure 4.2 Yield shear force coefficient (μ =3.0)

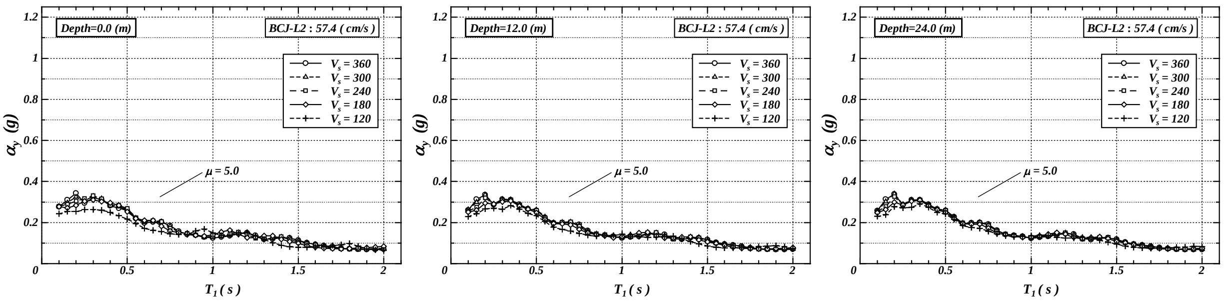

Figure 4.3.1 Depth=0(m) Figure 4.3.2 Depth=12(m) Figure 4.3.3 Depth=24(m)

Figure 4.3 Yield shear force coefficient (μ =5.0)

Yield Shear force Coefficient

Fig.4.1-4.2 show the yield shear force coefficients α_y at the inputting *BCJ-L2* wave motion. Those figures are corresponding to the setting maximum response ductility factors (μ = 1.5, 3.0 and 5.0) and embedment depths (depth = 0(m), 12(m) and 24(m)). Moreover, four kinds of ground shear wave velocity V_S are set to single upper-structure model.

In case where maximum response ductility factors μ is 1.5, within the short range of natural periods T_1, the response differences of α_y is large between the ground shear wave velocity V_S. Moreover, if the value of V_S increases, the changes by the natural period T_1 increases, too. On the other hand, in case where maximum response ductility factors μ are 5.0, the response differences of α_y between V_S become small. Furthermore, the changes by each natural period T_1 is smaller.

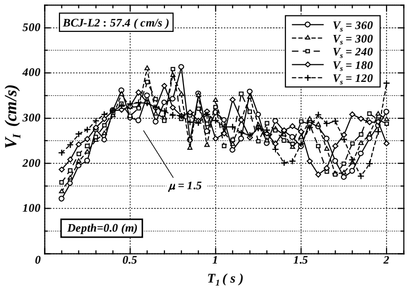

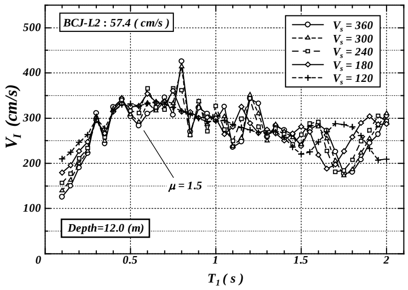

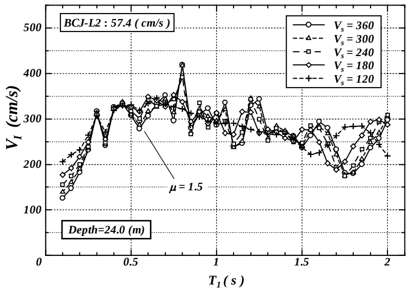

Figure 5.1.1 Depth=0(m) Figure 5.1.2 Depth=12(m) Figure 5.1.3 Depth=24(m)

Figure 5.1 Input energy equivalent velocity (μ =1.5)

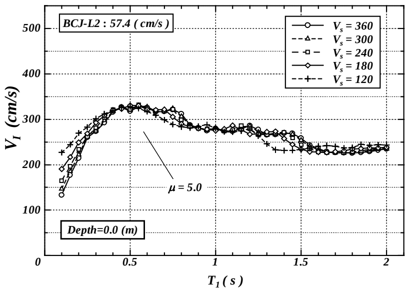

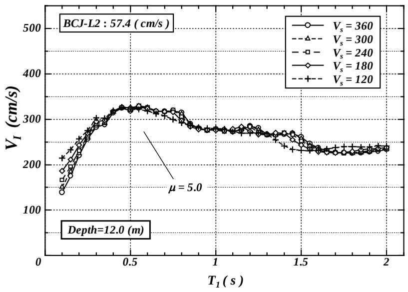

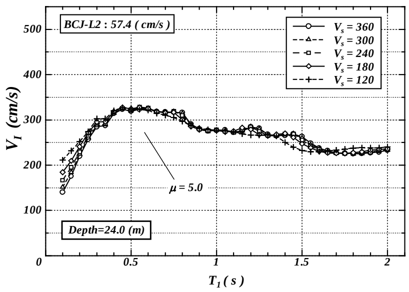

Figure 5.2.1 Depth=0(m) Figure 5.2.2 Depth=12(m) Figure 5.2.3 Depth=24(m)

Figure 5.2 Input energy equivalent velocity (μ =5.0)

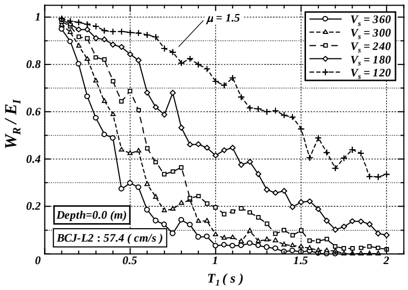

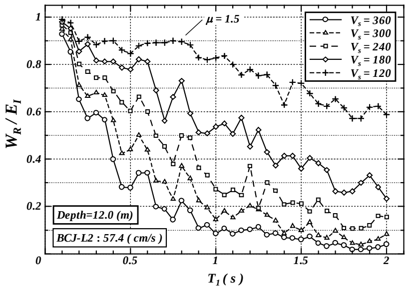

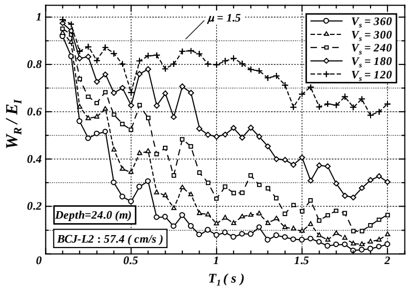

Figure 6.1.1 Depth=0(m) Figure 6.1.2 Depth=12(m) Figure 6.1.3 Depth=24(m)

Figure 6.1 Ratio of radiation damping (μ =1.5)

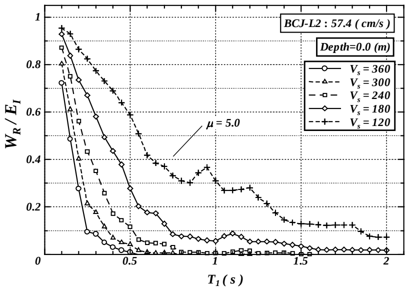

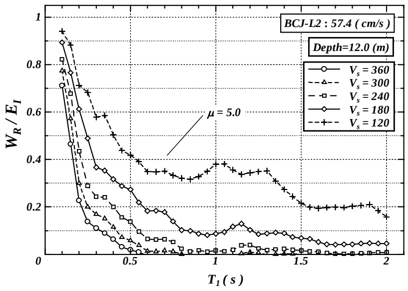

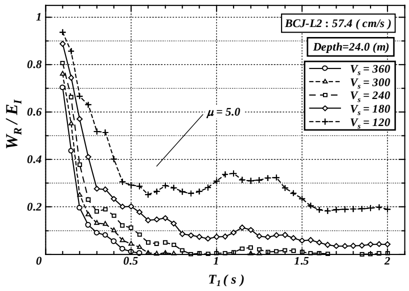

Figure 6.2.1 Depth=0(m) Figure 6.2.2 Depth=12(m) Figure 6.2.3 Depth=24(m)

Figure 6.2 Ratio of radiation damping (μ =5.0)

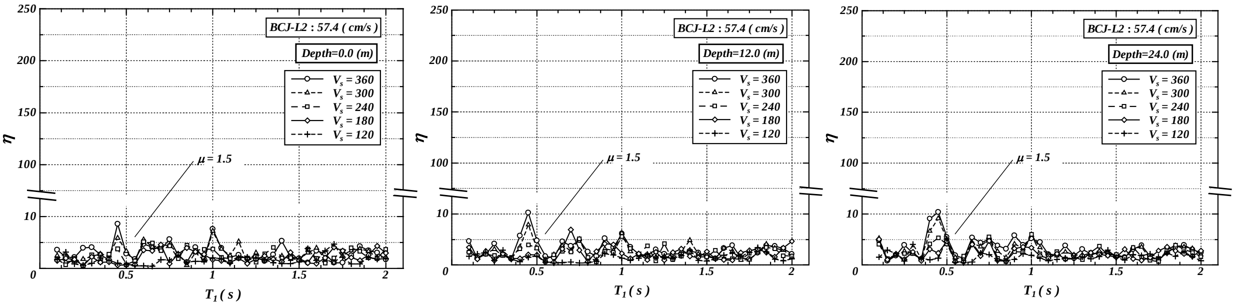

Figure 7.1 Cumulative plastic deformation (μ =1.5)

Figure 7.1.1 Depth=0(m) Figure 7.1.2 Depth=12(m) Figure 7.1.3 Depth=24(m)

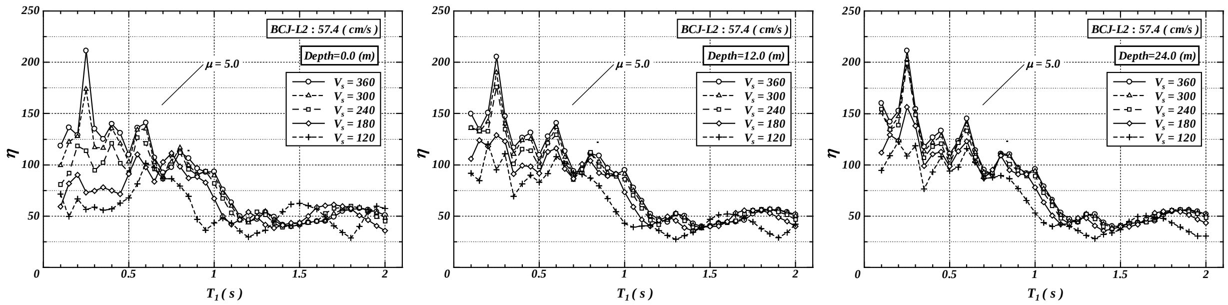

Figure 7.2.1 Depth=0(m) Figure 7.2.2 Depth=12(m) Figure 7.2.3 Depth=24(m)

Figure 7.2 Cumulative plastic deformation (μ =5.0)

Input Earthquake Energy

Fig. 5.1 and 5.2 show the input energy equivalent velocity V_I at each ground shear wave velocity V_S. Those figures are corresponding to the setting value of μ = 1.5 and 5.0 of embedment depth 0(m), 12(m) and 24(m) respectively.

When using μ = 1.5 structure models, differences of characteristics are little large at each ground shear wave velocity V_s. But the difference of response curve between μ = 1.5 and 5.0 upper-structure models is small and the difference between embedment depth is small, too. In addition, when using μ = 5.0 models, the change by T_1 is smoother than μ = 1.5 models.

Ground Radiation Damping Energy

Fig.6.1 and 6.2 show the consumption ratio of radiation damping energy W_R by inputting earthquake energy E_I at each ground shear wave velocity V_S. Those figures are corresponding to the setting value of μ = 1.5 and 5.0 of embedment depth 0(m), 12(m) and 24(m) respectively.

When using μ = 1.5 structure models, the ratios (W_R/E_I) become large as the first natural periods T_1 shorten and as the ground shear wave velocity V_s become small; at V_s = 120(m/s) and T_1 = 1.0(s) or less over about 80% of the input earthquake energy is consumed by radiation damping regardless of embedment depth. Moreover, when the value of μ is 5.0, at V_S = 120(m/s) and T_1 = 1.0(s) or less more than about 30% of input energy is consumed by radiation damping to soil ground.

Therefore, it is understood that dynamic soil-structure interaction considering embedment foundation is effective even for the high ductile structure (upper-structure of high energy-absorption performance) if it is a case when the value of V_S is small and the first natural period T_1 is short.

Cumulative Plastic Deformation

Fig.7.1 and 7.2 show the cumulative plastic deformation η of the upper-structure at each ground shear wave velocity V_S. Those figures are corresponding to the setting value of μ 1.5 and 5.0 of embedment depth 0(m), 12(m) and 24(m) respectively.

When using μ = 1.5 models, the change of η value is little regardless of the ground shear wave velocity V_S, the first natural period T_1 and the embedment depth, and the value is also extremely small. On the other hand, when using μ = 5.0 models, the value of η tends to decrease as the ground shear wave velocity becomes small regardless of embedment depth. Therefore, now, the effect of soil-structure interaction appears concerning the ground shear wave velocity V_S and the first natural period T_1.

From the above-mentioned, when the maximum response ductility factor μ of the upper-structure model is comparatively high, the effect of a dynamical soil-structure interaction appears at the cumulative plastic deformation that is the evaluation index of the structure aseismatic safety.

5. CONCLUDING REMARKS

Present study is concerned with examining seismic response properties in energy absorption foundation, when evaluating aseismic performance index of upper structure. The following remarks are obtained as valuable results.

(1) Dynamic soil-structure interaction effect is not seemed appreciable in case that the elasto-plastic behavior is obvious for upper-structure and when base foundation is embedded.

(2) Radiation damping effect is apparent in upper-structure from the consumption ratio of input quake energy when energy absorption performance is comparatively high, shear wave V_S is small and the first natural period T_1 is short.

(3) Seismic safety effect is remarkable with large amounts of cumulative plastic deformation such as maximum ductility factor μ to be highly 5.0. Therefore, the interaction phenomena greatly contribute to the improvement of aseismic performance even though upper structures are set to absorb seismic energy highly.

REFERENCES

1. Ito, S., Yamashita, T. and Inoue, Y. Aseismic effect on radiation damping for high ductility structures. *13th WCEE*, No.1538, 2004.
2. Kobori, T., Minai, R., Suzuki T. and K. Kusakabe. “Dynamical ground compliance of rectangular foundations on a semi-Infinite elastic medium, Part 1.” Annuals, Disas. Prev. Res. Inst.,Kyoto Univ., No.10A, 1967: 283-314. (in Japanese)
3. Kensuke Baba. Soil-structure interaction systems on the base of the ground impedance functions formed into a chain of impulses along the time axis. *11th WCEE*, No.1186, 1996.
4. Novak, M., Nogami, T. and Aboul-Ella, F. Dynamic Soil Reactions for Plane Strain Case. *J. of Engineering Mechanics, ASCE*, **Vol.104:No.EM4**, pp.953-959, 1978.
5. Yoshida, K. A comparative study on dynamic impedance functions for surface foundations on an elastic half space. *Journal of Structural and Construction Engineering (Transactions of AIJ)*, No.457, March 1994. (in Japanese)
6. Press WH, Teukolsky SA, Vetterling WT, Flannery BP. Numerical recipes in C – the art of scientific computing. Cambridge: Cambridge University Press, 1992.
7. Eduardo, M. Evaluation of site-dependent inelastic seismic design spectra. *Journal of Structurel Engineering, ASCE*, **Vol.119:No.5**, 1993: 1319-1337.